PHYSICS AND CHEMISTRY OF SOLID STATE
V. 21, No. 3 (2020) pp. 377-389

Vasyl Stefanyk Precarpathian National University

ФІЗИКА І ХІМІЯ ТВЕРДОГО ТІЛА
Т. 21, № 3 (2020) С. 377-389

DOI: 10.15330/pcss.21.3.377-389

PACS 61.66.Hq

ISSN 1729-4428

S. Sakthy Priya[1], K. Balakrishnan[1], A. Lakshmanan[1], P. Surendran[1], P. Rameshkumar[1], Karthik Kannan[2], P. Geetha[3], Tejaswi Ashok Hegde[4], G. Vinitha[4]

Crystal Growth and Characterization of Benzimidazolium Salicylate Single Crystal for Nonlinear Optical Studies and Antibacterial Activity

[1]*Periyar E. V. R. College (Autonomous), Affiliated to Bharathidasan University, Tiruchirappalli, Tamilnadu 620023, India, rameshkumarevr@gmail.com*
[2]*Center for Advanced Materials, Qatar University, PO Box 2713, Doha, Qatar, karthikkannanphotochem@gmail.com*
[3]*Quaid-E-Millath Government College for Women (Autonomous),Chennai 600002, Tamilnadu, India, geethasuresh29081978@gmail.com*
[4]*School of Advanced Sciences, Vellore Institute of Technology, Chennai, Tamilnadu 600127, India, tejaswihegade4@gmail.com*

Organic non-linear optical Benzimidazolium salicylate (BISA) single crystals have been harvested from methanol solution by slow evaporation method. The grown crystals belong to the monoclinic crystal system with space group P21/c. Good crystalline nature of grown BISA crystal was confirmed by PXRD. The FTIR spectrum analysis affirms the presence of functional groups in BISA crystal. From the UV–Vis-Absorption spectrum, the lower cut-off wavelength (356 nm) and its energy band gap and linear refractive index were calculated. Luminescence spectrum was recorded to explore the emission peak at 426 nm. The mechanical strength of BISA crystal was determined by Vickers microhardness tester and mechanical parameters like Elastic stiffness constant (C_{11}), Knoop hardness (H_k), Fracture toughness (K_c), and Brittleness index (B_i) were calculated for the first time. Dielectric properties of grown crystals were systematically investigated for different temperatures. Further, electronic polarizability (α) were calculated using Penn analysis and Clausius–Mossotti equation. Z–scan measurement was taken to explore the third-order NLO properties of BISA crystal and calculated values was found to be β (3.856×10^{-5} cm/W), n_2 (1.7882×10^{-9} cm^2/W), and $\chi^{(3)}$ (6.3088×10^{-7} esu). For the first attempt, the BISA crystals were tested against five human pathogenic bacterial, i.e. *Bacillus cereus, Staphylococcus aureus, Shigella flexneri, Vibrio cholerae,* and *Klebsiella pneumoniae*. Existing results established that Benzimidazolium salicylate crystals might find useful applications in nonlinear optics and antimicrobial field.

Keywords: crystal growth, optical studies, dielectric studies, Z-scan analysis, antibacterial activity.

Received 14 July 2020; Accepted 15 September 2020.

Introduction

Nonlinear optical compounds are significantly used in numerous applications such as image processing, electro-optical switching devices, telecommunications, optical information processing and optical data storage [1-4]. The researchers are motivated to find an efficient NLO material due to the demand of NLO crystals which are used in various fields [5]. The organic compounds typically have strong coulombic interactions between electron donor and acceptor group in the structure which have significant NLO efficiency [6]. Organic compounds have π-conjugated molecules which can be used in various applications such as organic LEDs, photorefractive devices, photovoltaics and waveguides however organic molecules are of low cost, low weight and flexible in nature [7, 8]. Organic NLO crystals have spectacular properties which motivated the researchers to find an alternate for the inorganic crystals due to their high nonlinear response and have good optical damage threshold [9, 10].

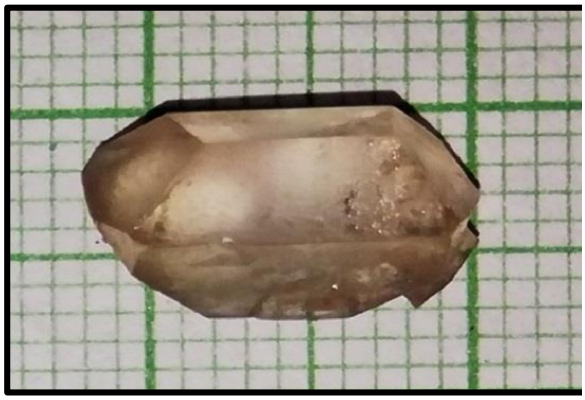

Fig. 1. As grown single crystal of Benzimidazolium salicylate.

Recent literature survey reveals that organic compounds like benzimidazole derivatives have been successfully developed in optical and medical applications, such as blue light emitting, optical limiting, antimicrobial, anticancer, antiviral, antiprotozoal agents, human cytomegalovirus and antifungals [11-14]. The bacterial resistance of simple organic acids is well established in the literature VIZ. cinnamic acid, veratric acid, sobric acid, caprylic acid [15]. The title compound, Benzimidazolium is one such π-donor- acceptor molecular compound; it can receive a donor (H^+) form salicylic acid. Previously, Amudha et al., [16] reported the crystal structure of Benzimidazolium Salicylate and also SHG conversion efficiency determined by Kurtz's Perry technique [17]. Jeyaram et al. has studied about the BISA for exploitation towards the NLO application below 118°C [18]. A detailed literature survey shows that no significant studies are available for this material.

Based on these facts, in this manuscript, we have studied the XRD, FTIR, UV–Visible absorption, Vickers microhardness studies, Luminescence, Dielectric analysis for different temperatures, Z–scan analysis and antibacterial activities which were performed for the grown BISA single crystal. The antibacterial study has been reported for the first time to confirm the effectiveness of the material in biological applications.

I. Experimental procedures

1.1. Material synthesis

The title compound Benzimidazolium salicylate (BISA) was synthesized by slow evaporation method. BISA single crystal was obtained by dissolving estimated amount (stoichiometric ratio) of Benzimidazole and salicylic acid in methanol at room temperature. After constant magnetic stirring for 6 hrs, the saturated solution was filtered in order to remove the impurities. Without any disturbance, the filtrate was allowed to evaporate in dust free atmosphere. As a result, at a time span of 10 days good quality single crystal was harvested. Fig. 1 shows the as grown BISA single crystal with dimension 12×8×7 mm^3. Fig. 2 shows the nucleation photograph of

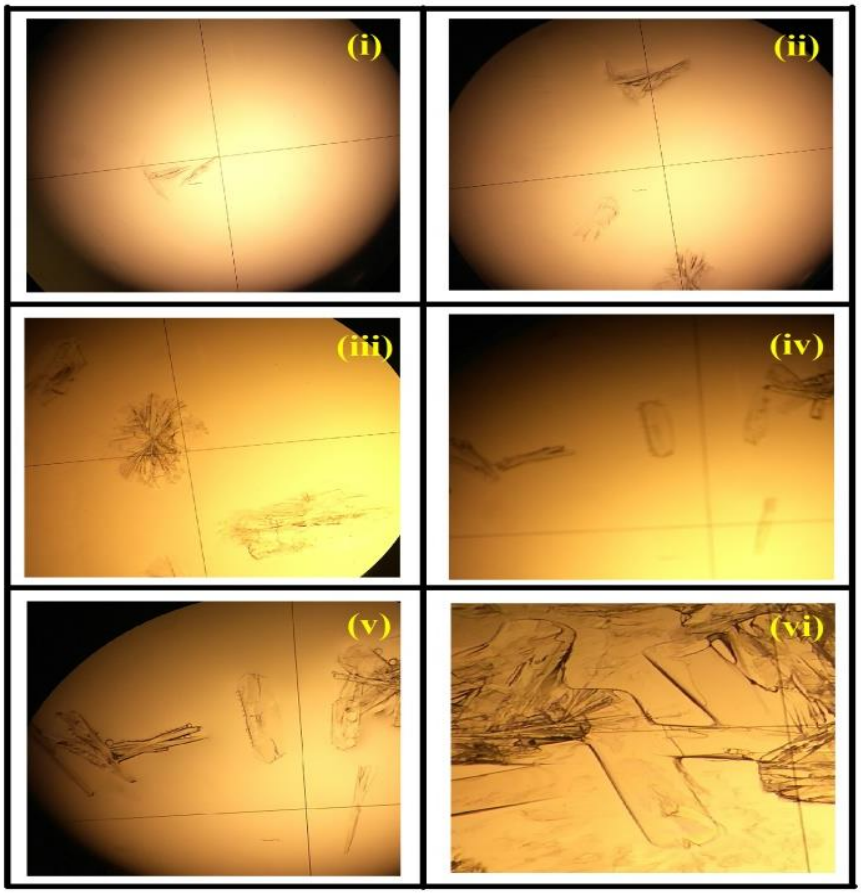

Fig. 2. Nucleation photograph of growth crystal BISA at different time interval (i) 5 sec, (ii) 10 sec, (iii) 15 sec, (iv) 20 sec, (v) 25 sec.

the grown crystal BISA at different time interval (i) 5 sec, (ii) 10 sec, (iii) 15 sec, (iv) 20 sec and (v) 25 sec.

$$C_7H_6N_2 + C_7H_6O_3 \rightarrow C_7H_7N_2^+ . C_7H_5O_3^-.$$

II. Results and discussion

The grown BISA crystal was finely powered and subjected to powder X–ray diffraction analysis to find the lattice parameters and crystalline nature of the sample. The recorded XRD pattern clearly defines sharp and strong peak which refers to high crystallinity of the crystal. The grown crystal crystallizes in *monoclinic* system (a = 7.4789 Å, b = 6.6808 Å, and c = 24.8908 Å) which was in good agreement with the reported [16]. The XRD pattern of BISA crystal is shown in Fig. 3. The corresponding peaks were indexed using checkcell software. The calculated average crystallite size is 41 nm. The microstrain (η) in the lattice of the crystal is calculated using Hall–Williamson equation:

$$\beta \cos\theta = \frac{K\lambda}{D} + 4\eta \, Sin\theta, \qquad (1)$$

where β, θ, K, λ and D are full width half maximum of diffraction peaks, Bragg's diffraction angle of the peaks, Scherrer constant, wavelength of X–ray and crystallite size. Fig. 4 shows the Williamson–Hall plot of BISA crystal and the strain value η is 7.612×10^{-4}. The positive strain indicates tensile strain which is due to defects in crystal lattice [19]. The properties of the crystal is influenced by dislocation density and can be calculated using

$$\delta = \frac{1}{D^2}. \qquad (2)$$

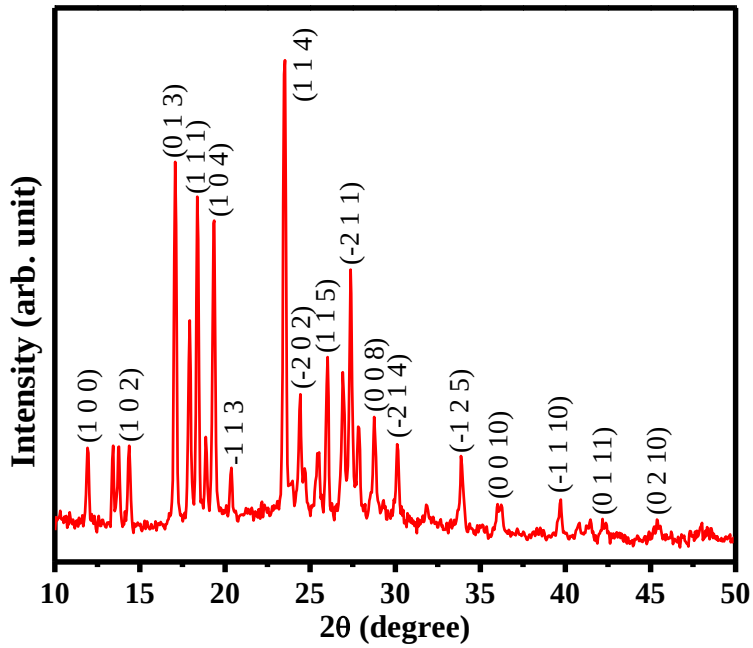

Fig. 3. XRD pattern of BISA crystal.

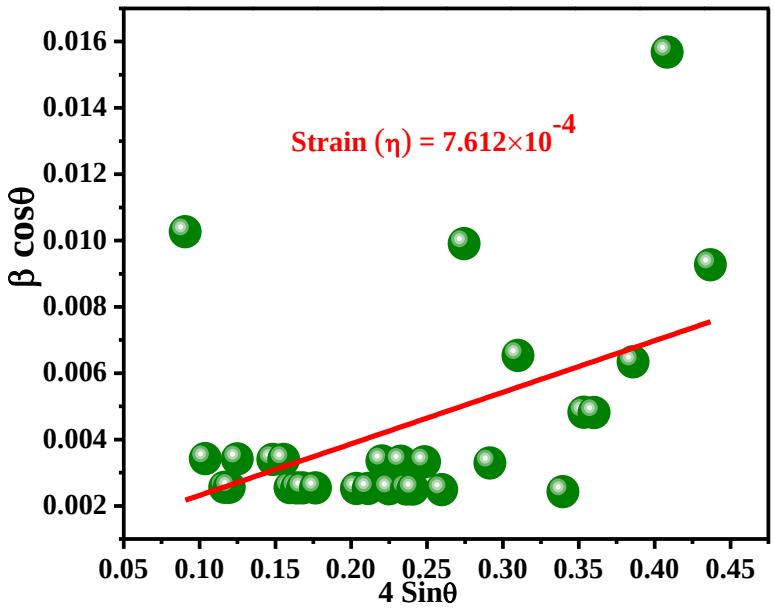

Fig. 4. Williamson–Hall plot of BISA crystal.

The calculated dislocation density value is 5.9488×10^{-14} (lines/m^2).

The FTIR spectrum of BISA crystal is shown in Fig. 5. In general, organic compounds present in the range 4000 to 1500 cm^{-1}. From the FTIR spectrum, it is evident that 3084 and 2989 cm^{-1} are due to asymmetric and symmetric C–H stretching vibration of aromatic ring. In free salicyclic acid, C=O vibration occur at 1750 cm^{-1} but here there is a shift towards low value at 1624 cm^{-1} which confirms the transfer of carboxylic proton to benzimidazole. The bands at 1591, 1479, 1452 and 1381cm^{-1} are assigned to aromatic C=O stretching vibration of benzimidazole [20]. The C–O carboxylate stretching is at 1244 cm^{-1}. Generally C–H out of plane and in plane bending vibration is observed at 950 to 600 cm^{-1} and 1300 to 1000 cm^{-1} respectively [21]. In this spectrum, 1142 cm^{-1} is attributed to C–H in plane bending and 766 cm^{-1} are for C–H out of plane bending of aromatic ring. The band at 1032 and 934 cm^{-1} are due to C–N stretching.

The UV-Vis spectrum gives information about the absorption of UV and visible light which involves in the transmission of electron in σ and π orbitals from the ground to the higher energy states [22, 23]. The optical absorption spectrum of BISA crystal is given in Fig. 6(a). It shows an absorption edge at 352 nm. Using standard calculation, the optical energy band gap can be calculated by equation:

$$(\alpha h\upsilon) = A(h\upsilon - E_g)^n, \quad (3)$$

where A is a constant, h is Planck's constant, E_g is band gap of the material, and exponent n depends on the type of transition in the sample. The parameter n has value of

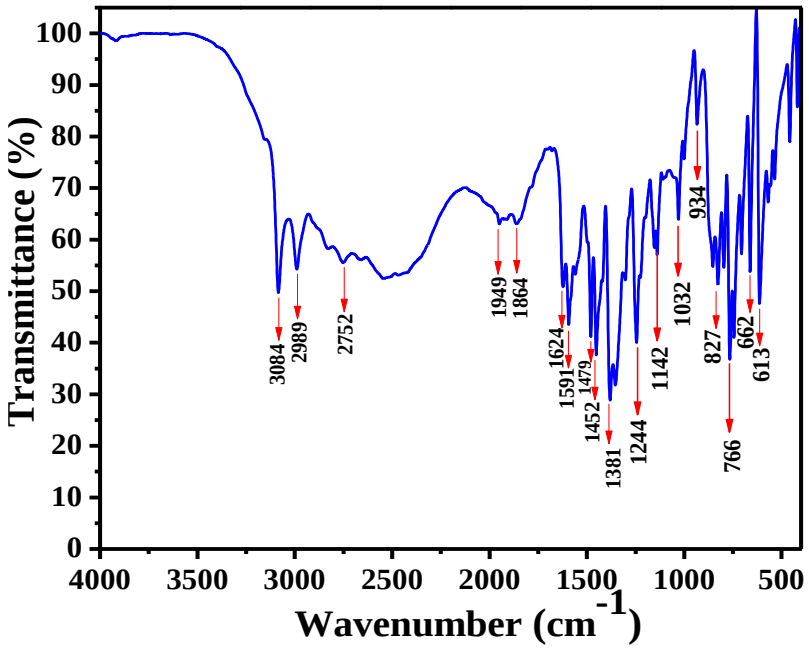

Fig. 5. FTIR spectrum of BISA crystal.

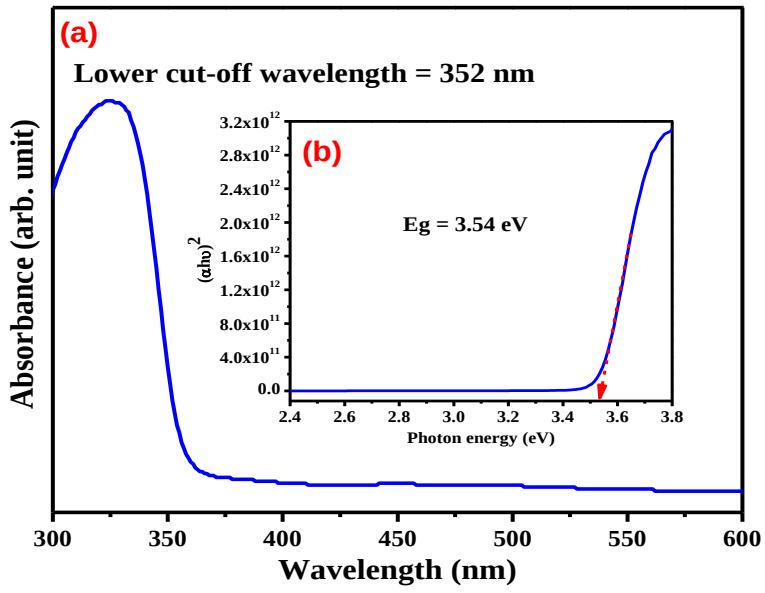

Fig. 6. (a) Optical absorption spectrum of BISA crystal (b) Tauc's plot between $(\alpha h\upsilon)^2$ *Versus* photon energy.

1/2 for direct transition and 2 for indirect transition. The tauc's plot between $(\alpha hv)^2$ *versus* Photon energy is plotted as shown in Fig. 6(b). The calculated optical energy band gap is 3.54 eV. The lower cut-off wavelength in visible region confirms that BISA crystal is suitable for optoelectronic applications. The reflectance (R) and refractive index (n_0) in terms of the absorption coefficient has been calculated using the expression [24]:

$$R = \frac{\exp(-\alpha t) \pm \sqrt{\exp(-\alpha t)T - \exp(-3\alpha t)T + \exp(-2\alpha t)T^2}}{\exp(-\alpha t) + \exp(-2\alpha t)T} \quad (4)$$

The linear refractive index (n_0) of the grown BISA crystal was calculated using the following equation [25]:

$$n_0 = -(R+1) \pm 2\frac{\sqrt{2}}{(R-1)}. \quad (5)$$

The calculated n_0 value is 1.23, it is used to calculate the third order nonlinearity $\chi^{(3)}$ of the BISA crystal.

The recorded luminescence spectrum of BISA crystal from the range of 300 to 600 nm is shown in Fig. 7. The excitation wavelength of the crystal is 352 nm which is within the UV region that shows good emission peak and confirms better luminescence behaviour [26, 27]. The luminescence spectrum has a broad spectrum with maximum intensity at 426 nm which corresponds to the blue emission. It is due to the electron donor NH_2 group and electron acceptor in COOH group present in the grown crystal [28]. No other additional peaks found in the spectrum which clearly shows that the whole energy is transferred into the intermolecular carboxylate ions [29]. Hence from luminescence analysis, it endorses that the BISA crystal can be used in blue LED applications.

The mechanical strength of BISA crystal was determined by Vickers microhardness measurement by choosing the smooth and flat face of the crystal. The crystal was placed on the base of the microscope. Using Vickers diamond pyramid indenter, the loads varying from 25 g to 100 g was indented for the dwell period of 10s. As the load was applied for different indentation, the two diagonal (d) lengths were measured and the average d was calculated. The microhardness number was estimated by standard relation;

$$H_v = 1.854 \times \frac{P}{d^2}(kg/mm^2). \quad (6)$$

Where P is the load applied (kg), d is the diagonal length of the indentation (mm) and Hv is the Vickers microhardness number (Kg/mm^2). Fig. 8 shows the variation of hardness number with load P. Above 100 g,

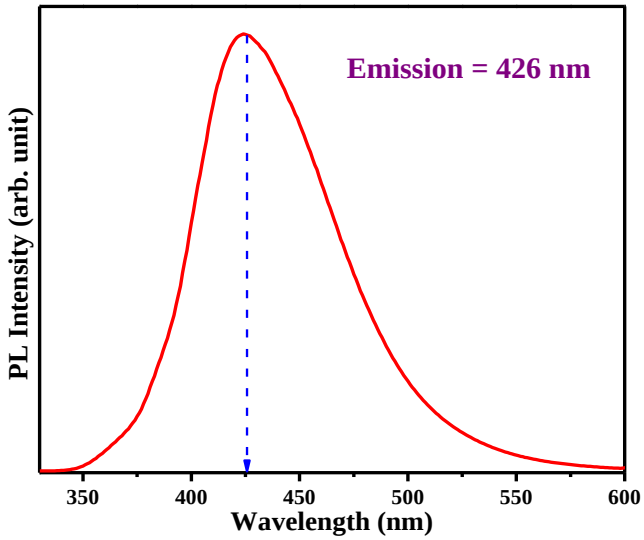

Fig. 7. Luminescence spectrum of BISA crystal.

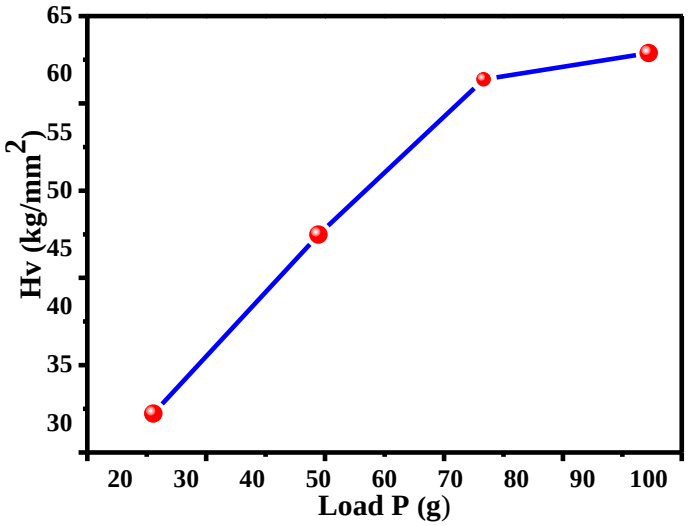

Fig. 8. Variation of hardness number with load P.

the crystal starts to crack during indentation due to the discharge of internal stress. Meyer's index was calculated by:

$$P = Kd^n, \quad (7)$$

$$\log P = \log k + n \log d. \quad (8)$$

Where k is material constant, n is Meyer's index. Using Meyer's relation it is clear that hardness number Hv increases with load P, when n>2 and Hv decreases with load P when n < 2. A graph is drawn between log P *versus* log d as shown in Fig. 9. From the graph, the work hardening coefficient is found to be 4.10. According to Onitch, [30] if 'n' is greater than 1.6 then the material is under soft material category which is useful for the fabrication of optoelectronic devices. The bond strength of the material can be determined by calculating elastic stiffness constant (C_{11}) for different loads using Wooster's empirical formula [31].

$$C_{11} = (H_v)^{7/4}. \quad (9)$$

The yield strength of the grown BISA crystal is calculated using the relation:

$$\sigma_y = \frac{H_v}{3}. \quad (10)$$

Fig. 10 shows the variation of yield strength with load P. The knoop hardness of the crystal can be calculated using the relation [32, 33]:

$$H_k = 14.229\left(\frac{P}{d^2}\right)\ (kg/mm^{-2}). \quad (11)$$

The fracture mechanism due to well-developed crack during indentation process [34,35] can be related by

$$K_c = \frac{P}{\beta_0 C^{3/2}}. \quad (12)$$

Where β_0 is 7 for Vickers indenter and C is the crack length of the crystal. This is due to the elastic stress field in the crystal during indentation. Brittle index is the relation between hardness number and fracture toughness which gives information about the fracture induced in the crystal.

$$B_i = \frac{H_v}{K_c}. \quad (13)$$

The calculated mechanical parameters are tabulated

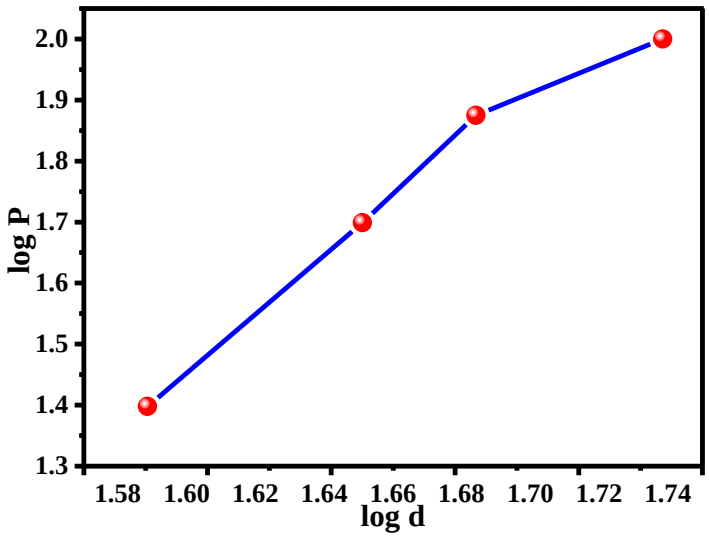

Fig. 9. Plot between log P *Vs* log d.

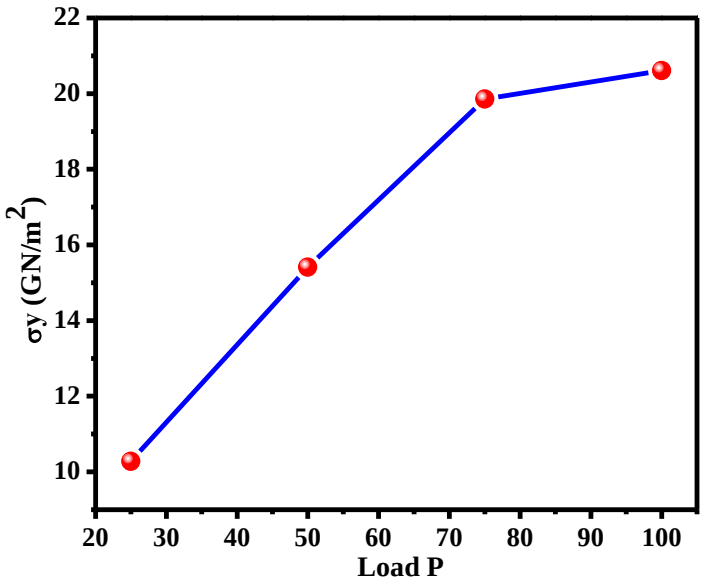

Fig. 10. Load (P) dependent yield strength (σ_y).

Table 1

Microhardness (H_v), stiffness constant (C_{11}), yield strength (σ_y), Knoop hardness (H_k), fracture toughness (K_c) and brittleness values (B_i) of BISA crystal

Load P (g)	H_v (kg/mm^2)	$C_{11} \times 10^{14}$ (Pa)	σ_y (GN/m^2)	H_k (kg/mm^2)	$K_c \times 10^4$ (kg/m$^{3/2}$)	B_i (μ/m$^{1/2}$)
25	30.8320	3.9561	10.2773	0.236628	0.009367	2.4353
50	46.2286	8.0371	15.4095	0.354794	0.018734	1.8250
75	59.5671	12.5250	19.8557	0.457164	0.028102	1.5679
100	61.8276	13.3684	20.6092	0.474512	0.037469	1.2204

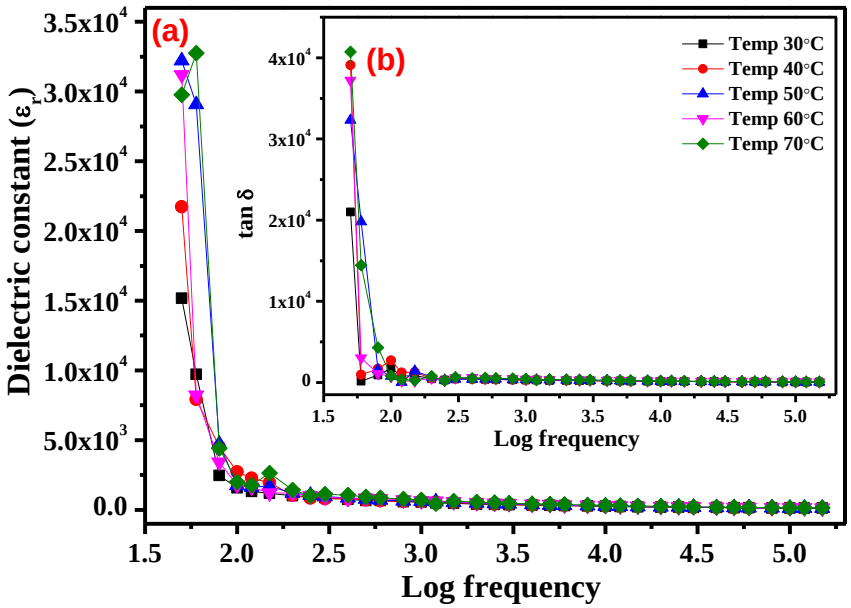

Fig. 11. (a) Plot of dielectric constant *versus* log frequency (b) tan δ Vs log frequency.

in Table 1.

To perform dielectric measurements, the response to an applied low ac voltage was made in the grown single crystal of BISA using the LCRZ meter as a function frequency between 50 Hz to 200 kHz at different temperature 30°- 70°C respectively. The dielectric constant (ε_r) for different frequency and temperature dependence of the BISA crystal is displayed in Fig. 11(a). These figures suggest that ε_r value decreases as the frequency increase and also ε_r increases with increase in temperature at low frequency. Temperature plays a role in determining the values of the dielectric constant. At higher temperatures, the dielectric constant is large and is attributed to the blocking of charge carriers at the electrodes. The dielectric loss (tanδ) is displayed in Fig. 11(b). From the figure, it can be understood that the dielectric loss is low at high frequency. The low dielectric loss value indicates that the grown BISA crystals are of good quality and have fewer defects/impurities. According to the Miller rule, the optimization of the SHG coefficient can be achieved by the lower value of dielectric constant. The calculation of the AC conductivity (σ_{ac}) was performed using the following expression [36, 37],

$$\sigma_{ac} = 2\pi f \varepsilon_r \varepsilon_0 \tan\delta, \qquad (14)$$

where ε_0 is the permittivity of free space and f is the applied frequency (Hz). The deviation of AC conductivity with applied frequency is depicted in Fig. 12.

The electronic polarizability (α) is the significant factor for the desired effect of optical nonlinearity. There are many theoretical approaches available to calculate the electronic polarizability of molecule such as Penn analysis, Clausius-Mossotti relation, and optical band gap. The electronic polarizability of grown BISA single crystal was calculated using dielectric constant at higher frequency (ε_r = 115.828 at 200 kHz) for room temperature. From the experimental values of the dielectric analysis, it is found that the dielectric constant is high due to valence electron plasma energy, Penn gap, Fermi energy and electronic polarizability [38]. The density of the sample is calculated by

$$\rho = \frac{MZ}{N_A V}, \qquad (15)$$

where M is the molecular weight of BISA (256.25 g/mol), Z is the molecular unit cell (Z = 4), N_A is the Avogadro number (6.023×10^{23}) and V is the volume of unit cell (4). The valence electron plasma energy can be calculated by

$$\hbar\omega_\rho = 28.8\sqrt{\frac{(Z\times\rho)}{M}}. \qquad (16)$$

The total number of valence electron of BISA crystal is Z = (14×4) + (12×1) + (2×5) + (3×6) = 96 where valence electron of C, H, N and O are 4, 1, 5 and 6 and ρ is the density. According to Penn model the average Penn gap and Fermi energy is calculated using the following equation [39, 40],

$$E_P = \frac{\hbar\omega_\rho}{\sqrt{\varepsilon_r - 1}};\ E_F = 0.2948(\hbar\omega_p)^{4/3}. \quad (17)$$

Electronic polarizability (α) of the crystal can be calculated by

$$\alpha = \left[\frac{(\hbar\omega_\rho)^2 s_0}{(\hbar\omega_\rho)^2 s_0 + 3E_P^2}\right] \times \frac{M}{\rho} \times 0.369 \times 10^{-24} cm^3, \quad (18)$$

where $s_0 = 1 - \left[\frac{E_P}{4E_F}\right] + \frac{1}{3} + \left[\frac{E_P}{4E_F}\right]^2$.

The electronic polarizability (α) is also confirmed and calculated by Clausius-Mosotti relation,

$$\alpha = \frac{3M}{4\pi N_A \rho}\left(\frac{\varepsilon_r - 1}{\varepsilon_r + 2}\right). \quad (19)$$

In addition, the value of electronic polarizability (α) can be obtained using the optical band gap given by,

$$\alpha = \left[1 - \frac{\sqrt{E_g}}{4.06}\right] \times \frac{M}{\rho} \times 0.396 \times 10^{-24} cm^3. \quad (20)$$

Where E_g is BISA crystal optical band gap (eV). The calculated solid state parameters of the title compound are tabulated in Table 2.

The Z–scan analysis is a sensitive single beam technique which is used to measure the optical nonlinearity of the crystal by moving the sample through the focus of Gaussian beam and detected the farfield sample transmittance with the function of sample position [3]. Recently materials which have high values of nonlinear optical parameters like nonlinear refractive index and nonlinear absorption coefficient are used to fabricate high speed optical devices [41]. Using closed aperture, the sign and magnitude of the nonlinear refractive index (n_2) can be evaluated and to calculate the nonlinear absorption coefficient (β) of the crystal, the open aperture Z-scan data was employed [42].

In the experiment CW laser (532 nm) of laser energy 100 mW was used to measure the nonlinear optical properties of the crystal. BISA defect free crystal was placed in the sample holder and moved along –Z to +Z direction parallel to the propagation of laser. A detector is used to collect the transmitted intensity which relies on the refractive index and absorption nature of the crystal. A lens is placed in front of the detector to collect the intensity which is used to calculate the nonlinear absorption coefficient (β). To find the nonlinear refraction (n_2) of the crystal, a aperture of radius

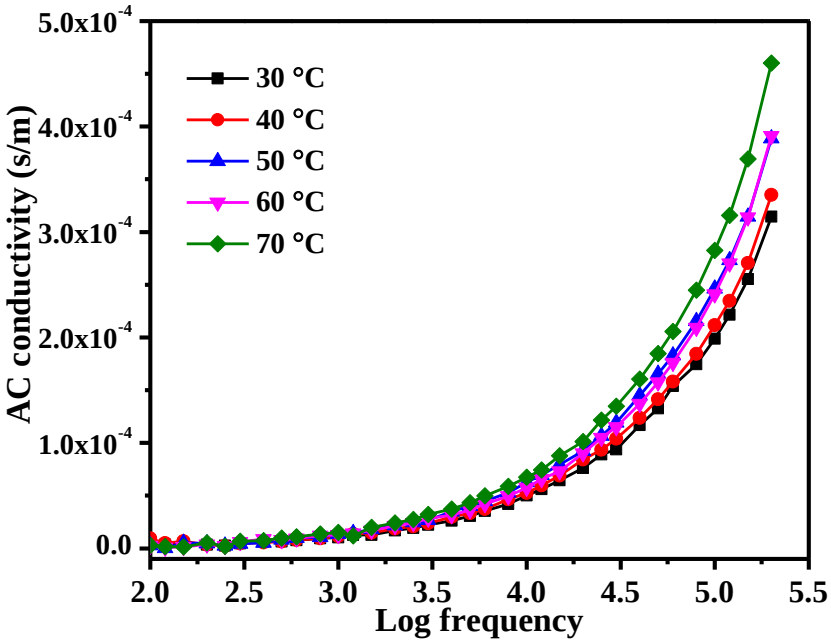

Fig. 12. AC conductivity as a function log frequency

Table 2

Polarizability (α) parameters of BISA single crystal

Parameters	Values
Molecular weight	256.25 (g/mol)
Density	1.3682 (g/cm^{-3})
Plasma energy	20.6191 (eV)
Penn gap	1.9241 (eV)
Fermi energy	16.6513(eV)
Electronic polarizability (α)	
From Penn analysis	7.22 × 10^{-23} cm^3
From Clausius–Mossotti equation	7.24 × 10^{-23} cm^3
From energy band gap	3.98 × 10^{-23} cm^3

1.25 mm is placed between the lens and detector. Fig. 13 and 14 shows the open and closed aperture of BISA crystal. In closed aperture (Fig. 13) peak is followed by valley which indicates negative nonlinear refractive index which is due to the self-defocusing nature [43]. In open aperture (Fig. 14) show valley in the data which exhibit strong reverse saturable absorption that confirms positive nonlinear absorption coefficient [44]. The nonlinear refractive is calculated by

$$n_2 = \frac{\Delta\phi}{KI_0L_{eff}}. \quad (21)$$

Here the wavenumber K is $2\pi/\lambda$, (λ is the wavelength of CW laser), I_o is the on-axis irradiation at the focus (Z = 0), $L_{eff} = \frac{(1-e^{-\alpha L})}{\alpha}$, L_{eff} is the effective thickness of the sample. The nonlinear absorption coefficient β was calculated using relation,

$$\beta = \frac{2\sqrt{2}\Delta T}{I_oL_{eff}}. \quad (22)$$

The real and imaginary parts of the third-order nonlinear optical susceptibility $\chi^{(3)}$ were calculated using the relation,

$$R_e(\chi^{(3)}) = \frac{10^{-4}\varepsilon_o c^2 n_o^2 n_2}{\pi} \text{ (cm}^2\text{/W)} \quad (23)$$

$$I_m(\chi^{(3)}) = \frac{10^{-2}\varepsilon_o c^2 n_o^2 \lambda\beta}{4\pi^2} \text{ (cm}^2\text{/W)}. \quad (24)$$

Where ε_o is the vacuum permittivity (8.854×10^{-12} F/m), C is velocity of light, n_o is linear refractive index of sample. The following equation is used to calculate the third order nonlinear optical susceptibility of the crystal,

$$\chi^{(3)} = \sqrt{(R_e\chi^{(3)})^2 + (I_m\chi^{(3)})^2}. \quad (25)$$

The third order susceptibility $\chi^{(3)}$ of BISA is 6.3088×10^{-7} *esu*. BISA crystal confirms the suitability in optical night vision sensing device due to negative

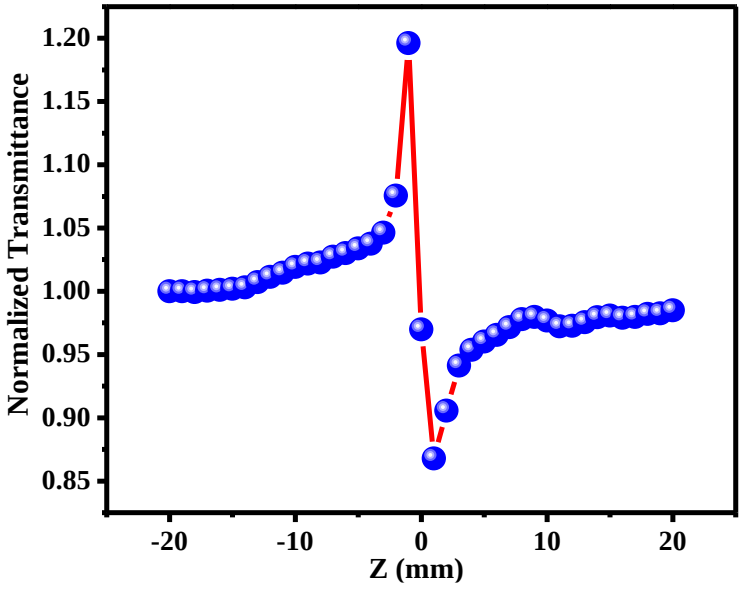

Fig. 13. Closed aperture Z-scan curve of BISA crystal.

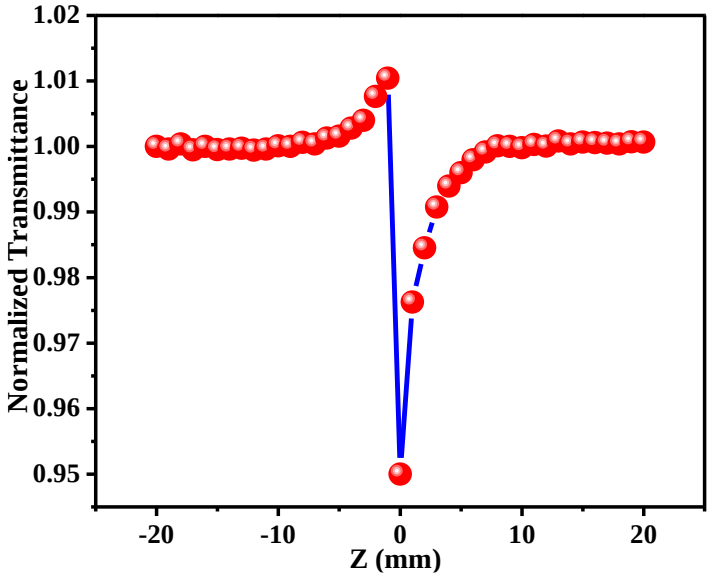

Fig. 14. Open aperture Z-scan curve of BISA crystal.

refractive index. The calculated remarkable values are because of the presence of delocalized π electronic configuration and effective intra molecular charge transfer interactions. The table 3 summarizes the values of the nonlinear indices, the nonlinear absorption coefficient and third order susceptibility of the crystal.

The antibacterial activity was performed for the grown crystals against gram positive *(Bacillus cereus, Staphylococcus Aureus*) and gram negative bacteria (*Shigella flexneri, Vibrio cholera* and *Klebsiella pneumonia*) by agar diffusion method. In general it is known that, if the zone of inhibition is greater than 6 mm, the sample has good antibacterial activity but if the zone of inhibition is less than 6 mm, the antibacterial activity is weak [45].

The antibacterial activity of the sample depends on reactive oxygen species (ROS), specific surface area, morphology, and raise in oxygen vacancies. ROS generation has notable biological importance. The ROS like super oxide anion radical (O_2), hydroxyl radical (OH), singlet oxygen ($1O_2$) and hydrogen peroxide (H_2O_2) can damage organic biomolecules like carbohydrates, nucleic acids, lipids, proteins, DNA and amino acids. The most oxidizing agent among ROS are H_2O_2 and OH radical, which will penetrate into the bacterial cell wall membrane and prevent the growth of cells and result in cell death [46-51].

From FTIR analysis, the generation of hydroxyl radical and the presence of hydrogen interaction in the title compound increases the efficiency of the antibacterial activity against the bacterial strains [52]. And from luminescence spectrum, the emission wavelength at 449, 467 nm are due to oxygen vacancies leading to higher number of ROS which is responsible for cell death [53, 54]. Fig. 15 shows disc photograph of the grown crystal which directly acts on the bacteria.

Table 3

Third–order (NLO) parameters of the grown BISA crystal

Third–order NLO parameters	Values
Linear refractive index (n_0)	1.23
Linear absorption coefficient (α)	93.189
Nonlinear refractive index (n_2) × 10^{-9} (cm^2/W)	1.78828
Nonlinear absorption coefficient (β) × 10^{-5} (cm/W)	3.856
Real part of the third–order (NLO) susceptibility (Re $\chi^{(3)}$) × 10^{-8} (esu)	6.86592
Imaginary part of the third–order (NLO) susceptibility (Im $\chi^{(3)}$) × 10^{-7} (esu)	6.27133
Third–order (NLO) susceptibility ($\chi^{(3)}$) × 10^{-7} (esu)	6.30881

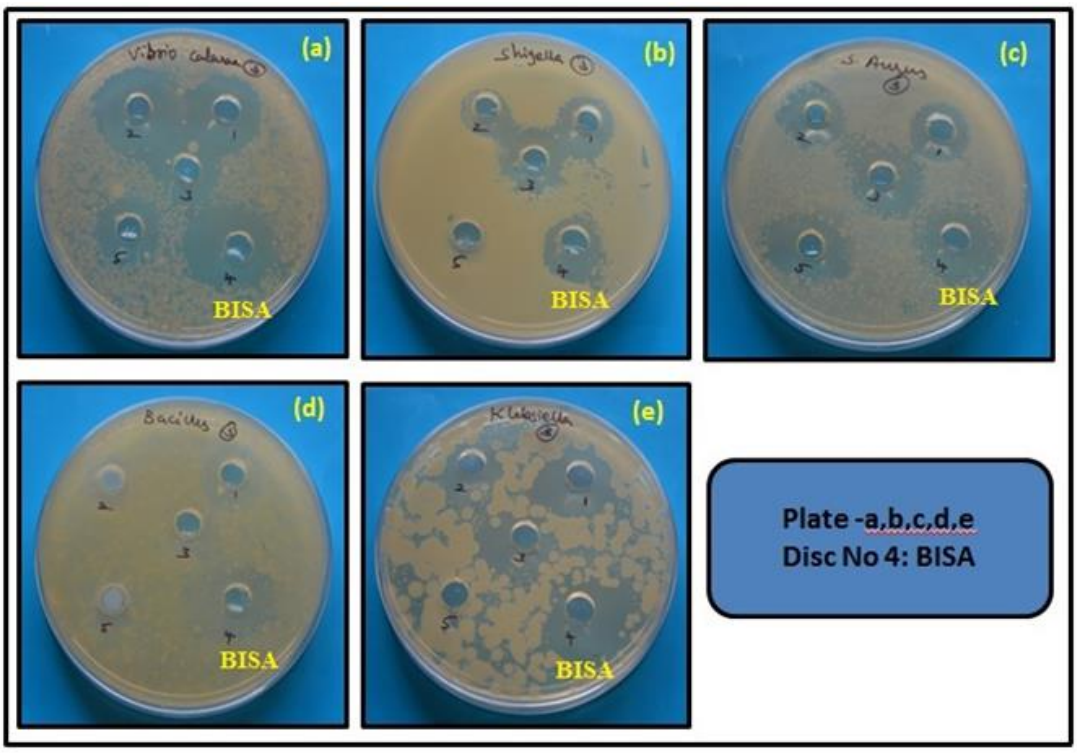

Fig. 15. Photographs of antibacterial plates of BISA crystal (a) *Vibrio cholerae* (b) *Shigella flexneri* (c) *Staphylococcus aureus* (d) *Bacillus cereus* and (*e*) *Klebsiella pneumoniae.*

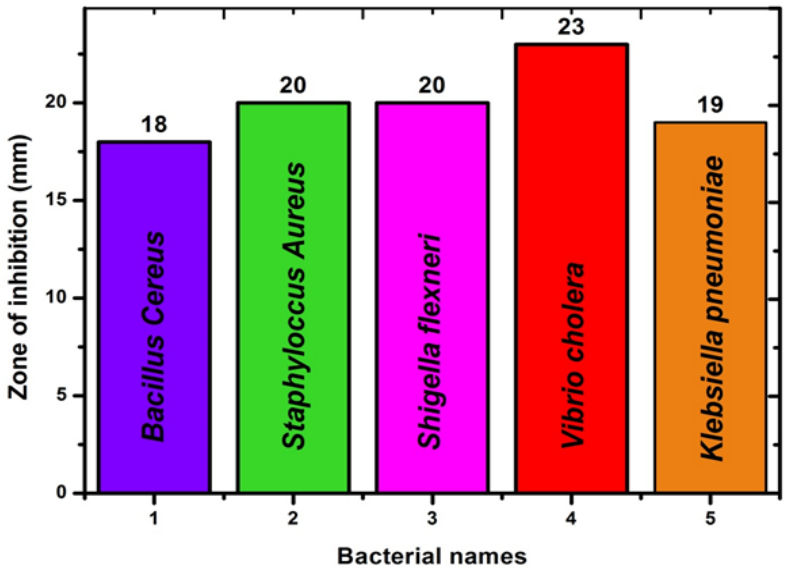

Fig. 16. Bar diagram for the selected bacterial strains.

From bar diagram (Fig. 16), it shows that BISA crystal has good antibacterial activity as the zone of inhibition is larger than 6 mm. Hence BISA crystal will be a potential candidate for the development of antibiotic drugs against tested pathogens.

Conclusions

An efficient organic nonlinear optical Benzimidazolium salicylate (BISA) single crystal was grown through slow evaporation method at ambient condition and was characterized by XRD which confirms centrosymmetric *monoclinic* system. The dislocation density and microstrain of the grown crystal was determined by W–H plot. The presence of various functional groups in the title compound was acknowledged by FTIR. From the UV–Vis absorption studies, the optical energy band of 3.54 eV and lower–cut of wavelength at 356 nm. Luminescence analysis revealed that the BISA crystal could be potential candidate in LED applications. Hardness measurement indicates that the BISA crystal possesses high mechanical strength and the grown crystal exhibits under soft material category. The frequency and temperature dependent dielectric behaviour was exhibited by BISA crystal, and it can be utilized in high frequency device applications. From the Z-scan analysis the grown BISA crystal indicates negative nonlinear refractive index which is due to the self–defocusing nature and the nonlinear absorption is observed as reverse saturable absorption which is most desirable property for optical night vision device and third-order NLO applications. Moreover, the grown BISA crystal also performs as a good antibacterial agent against human bacterial pathogens.

Acknowledgements

The author's A. L would like to thank, UGC-RGNF [F1-2016-17/RGNF 17.1/ -2015-17-SC-TAM-21802] India, and P. S acknowledge the financial support from UGC-NFHE [F1-17.1/2015-16/NFST-2015-17-ST-TAM-1335], India.

S. Sakthy Priya - Ph.D Research Scholar;
K. Balakrishnan - Ph.D Research Scholar;
A. Lakshmanan - Ph.D Research Scholar;
P. Surendran - Ph.D Research Scholar;
P. Rameshkumar - Assistant Professor;
Karthik Kannan – Ph.D in Physics, Research Fellow;
P. Geetha - Assistant Professor;
Tejaswi Ashok Hegde - Ph.D Research Scholar;
G. Vinitha - Assistant Professor.

[1] J. Arumugam, M. Selvapandiyan, S. Chandran, M. Srinivasan, P. Ramasamy, Mater Chem Phys 242, 122479 (2020) (doi:10.1016/j.matchemphys.2019.122479).
[2] M. Saravanakumar, J. Chandrasekaran, M. Krishnakumar, B. Babu, G. Vinitha, M. Anis, J Phys Chem Solids 136, 109133 (2020) (doi:10.1016/j.jpcs.2019.109133).
[3] P. Era, R.M. Jauhar, P. Murugakoothan, Opt Mater (Amst) 99, 109558 (2020) (doi:10.1016/j.optmat.2019.109558).
[4] S. Suresh, V. Jaisankar, G. Vinitha, R.M. Kumar, J Mol Struct. 1202, 127257 (2020) (doi:10.1016/j.molstruc.2019.127257).
[5] S.E. Allen Moses, S. Tamilselvan, S.M. Ravi Kumar, G. Vinitha, T.A. Hegde, G.J. Shanmuga Sundar, M. Vimalan, S. Sivaraj, J. Mater. Sci. Mater. Electron. 30, 9003 (2019) (doi:10.1007/s10854-019-01229-9).

[6] P. Antony, S.J. Sundaram, J.V. Ramaclus, S. Antony Inglebert, A. Antony Raj, S. Dominique, T.A. Hegde, G. Vinitha, P. Sagayaraj, J. Mol. Struct. 1196, 699 (2019) (doi:10.1016/j.molstruc.2019.07.024).
[7] S. Guidara, S. Elleuch, Y. Abid, H. Feki, J. Lumin. 178, 425 (2016) (doi:10.1016/j.jlumin.2016.06.030).
[8] S. John Sundaram, J.V. Ramaclus, M. Panneerselvam, M. Jaccob, P. Antony, L. Anandaraj, S. Muthupandi, A.J.P. Paul Winston, P. Sagayaraj, Opt. Laser Technol. 121, 105831 (2020) (doi:10.1016/j.optlastec.2019.105831).
[9] S.E. Allen Moses, S. Tamilselvan, S.M. Ravi Kumar, G. Vinitha, T.A. Hegde, M. Vimalan, S. Varalakshmi, S. Sivaraj, Mater. Sci. Energy Technol. 2, 565 (2019) (doi:10.1016/j.mset.2019.05.003).
[10] C.W. Ghanavatkar, V.R. Mishra, N. Sekar, E. Mathew, S.S. Thomas, I.H. Joe, J. Mol. Struct. 1203, 127401 (2020) (doi:10.1016/j.molstruc.2019.127401).
[11] L. Brulikova, J. Hlavac, Beilstein J. Org. Chem. 7, 678 (2011) (doi:10.3762/bjoc.7.80).
[12] A. Kantouch, A.A. El-Sayed, M. Salama, A.A. El-Kheir, S. Mowafi, Int. J. Biol. Macromol. 62, 603 (2013) (doi:10.1016/j.ijbiomac.2013.09.021).
[13] B. Narasimhan, D. Sharma, P. Kumar, Med. Chem. Res. 21, 269 (2012) (doi:10.1007/s00044-010-9533-9).
[14] S. Tahlan, S. Kumar, B. Narasimhan, BMC Chem. 13, 101 (2019) (doi:10.1186/s13065-019-0625-4).
[15] A. Khatkar, A. Nanda, P. Kumar, B. Narasimhan, Arab. J. Chem. 10, S3804 (2017) (doi:10.1016/j.arabjc.2014.05.018).
[16] M. Amudha, P.P. Kumar, G. Chakkaravarthi, Acta Crystallogr. Sect. E Crystallogr. Commun 71, o794 (2015) (doi:10.1107/S2056989015017764).
[17] M. Amudha, R. Rajkumar, V. Thayanithi, P. Praveen Kumar, Adv. Opt. Technol. 2015, 1 (2015) (doi:10.1155/2015/206325).
[18] J. Jeyaram, K. Varadharajan, B. Singaram, R. Rajendhran, J. Sci. Adv. Mater. Devices 2, 445 (2017) (doi:10.1016/j.jsamd.2017.09.004).
[19] A. Alexandar, P. Surendran, S. Sakthy Priya, A. Lakshmanan, P. Rameshkumar, J. Nonlinear Opt. Phys. Mater. 25, 1650037 (2016) (doi:10.1142/S0218863516500375).
[20] N. Vijayan, R. Ramesh Babu, R. Gopalakrishnan, P. Ramasamy, W.T.A. Harrison, J. Cryst. Growth 262, 490 (2004) (doi:10.1016/j.jcrysgro.2003.08.082).
[21] R.M. Silverstein, F.X. Webster, D.J. Kiemle, Spectrometric Identification of Organic Compounds, 7th editio John Wiley & Sons, INC., (2005).
[22] H.J.L. Hilary, P. Dhamodharan, P.C.J. Prabakar, A.C. Ferdinand, S. Thiyagaraj, N. Moorthy, Phys. B Condens. Matter 567, 25 (2019) (doi:10.1016/j.physb.2019.04.027).
[23] C. Sekar, R. Parimaladevi, Spectrochim. Acta Part A Mol. Biomol. Spectrosc. 74, 1160 (2009) (doi:10.1016/j.saa.2009.09.026).
[24] K. Senthil, S. Kalainathan, A.R. Kumar, P.G. Aravindan, RSC Adv. 4, 56112 (2014) (doi:10.1039/C4RA09112D).
[25] P. Surendran, A. Lakshmanan, G. Vinitha, G. Ramalingam, P. Rameshkumar, Luminescence 35, 196 (2020) (doi:10.1002/bio.3713).
[26] J. George, D. Sajan, J. Alex, A. Aravind, G. Vinitha, R. Chitra, Opt. Laser Technol. 105, 207 (2018) (doi:10.1016/j.optlastec.2018.02.056).
[27] M. Kalidasan, K. Baskar, R. Dhanasekaran, Curr. Appl. Phys. 16, 1113 (2016) (doi:10.1016/j.cap.2016.06.013).
[28] S. Chandran, R. Paulraj, P. Ramasamy, Opt. Mater. (Amst). 52, 49–55 (2016) (doi:10.1016/j.optmat.2015.11.044).
[29] M. Dhavamurthy, G. Peramaiyan, M. Nizam Mohideen, S. Kalainathan, R. Mohan, J. Nonlinear Opt. Phys. Mater. 24, 1550045 (2015) (doi:10.1142/S0218863515500459).
[30] E. M. Onitsch, Uber die Mikroharte der Metalle, Mikroscopia. 2, 131 (1947).
[31] K. Naseema, S. Ravi, R. Sreedharan, Chinese J. Phys. 60, 612 (2019) (doi:10.1016/j.cjph.2019.05.037).
[32] S. Jeeva, S. Muthu, G. Ganesh, K. Arulaabaranam, S. Chithra, P. Purushothaman, G. Vinitha, G. Mani, Chem. Data Collect. 19, 100169 (2019) (doi:10.1016/j.cdc.2018.11.011).
[33] V. Sangeetha, K. Gayathri, P. Krishnan, N. Sivakumar, N. Kanagathara, G. Anbalagan, J. Cryst. Growth 389, 30 (2014) (doi:10.1016/j.jcrysgro.2013.11.026).
[34] C. Ramki, R.E. Vizhi, Mater. Chem. Phys. 223, 230 (2019) (doi:10.1016/j.matchemphys.2018.10.034).
[35] A. Kelly, W.R. Tyson, A.H. Cottrell, Philos. Mag. A J. Theor. Exp. Appl. Phys. 15, 567 (1967) (doi:10.1080/14786436708220903).
[36] P. Thomas, S.D. Dhole, G.P. Joseph, Nucl. Inst. Methods Phys. Res. Sect. B Beam Interact. with Mater. Atoms 426, 46 (2018) (doi:10.1016/j.nimb.2018.04.005).
[37] R. Sathishkumar, S. Tamilselvan, C.J. Magesh, K. Venkatapathy, M. Vimalan, G. Lavanya, J. Mater. Sci. Mater. Electron. 30, 17504 (2019) (doi:10.1007/s10854-019-02102-5).
[38] S. Sakthy Priya, A. Alexandar, P. Surendran, A. Lakshmanan, P. Rameshkumar, P. Sagayaraj, Opt. Mater. (Amst). 66, 434 (2017) (doi:10.1016/j.optmat.2017.02.041).
[39] D.R. Penn, Phys. Rev. 128, 2093 (1962) (doi:10.1103/PhysRev.128.2093).
[40] R.G. Pearson, J. Chem. Educ. 45, 581 (1968) (doi:10.1021/ed045p581).

[41] S. Vediyappan, R. Arumugam, K. Pichan, R. Kasthuri, S.P. Muthu, R. Perumal, Appl. Phys. A 123, 780 (2017) (doi:10.1007/s00339-017-1394-3).
[42] A. Priyadharshini, S. Kalainathan, Opt. Mater. (Amst). 78, 35 (2018) (doi:10.1016/j.optmat.2018.02.017).
[43] G. Rajasekar, M.K. Dhatchaiyini, G. Vinitha, A. Bhaskaran, J. Mol. Struct. 1177, 594 (2019) (doi:10.1016/j.molstruc.2018.07.113).
[44] S.P. Ramteke, M.I. Baig, M. Shkir, S. Kalainathan, M.D. Shirsat, G.G. Muley, M. Anis, Opt. Laser Technol. 104, 83 (2018) (doi:10.1016/j.optlastec.2018.02.018).
[45] K. Karthik, S. Dhanuskodi, C. Gobinath, S. Prabukumar, S. Sivaramakrishnan, J. Phys. Chem. Solids 112, 106 (2018) (doi:10.1016/j.jpcs.2017.09.016).
[46] V. Vijayalakshmi, P. Dhanasekaran, N.M. Ganesan, Mol. Cryst. Liq. Cryst. 664, 241 (2018) (doi:10.1080/15421406.2018.1473994).
[47] K. Karthik, M.P. Nikolova, A. Phuruangrat, S. Pushpa, V. Revathi, M. Subbulakshmi, Mater. Res. Innov. 0, 1 (2019) (doi:10.1080/14328917.2019.1634404).
[48] V. Vijayalakshmi, P. Dhanasekaran, J. Cryst. Growth 498, 372 (2018) (doi:10.1016/j.jcrysgro.2018.07.013).
[49] V. Revathi, K. Karthik, J. Mater. Sci. Mater. Electron. 29, 18519 (2018) (doi:10.1007/s10854-018-9968-1).
[50] K. Kannan, D. Radhika, M.P, Nikolova, K.K, Sadasivuni, H. Mahdizadeh, U. Verma, Inorg. Chem. Commun. 113, 107755 (2020) (doi:10.1016/j.inoche.2019.107755).
[51] K. Karthik, S. Dhanuskodi, C. Gobinath, S. Prabukumar, S. Sivaramakrishnan, J. Mater. Sci. Mater. Electron. 28, 16509 (2017) (doi:10.1007/s10854-017-7563-5).
[52] M.T. Elakkiya, K. Anitha, Mater. Lett. 235, 202 (2018) (doi:10.1016/j.matlet.2018.10.015).
[53] K. Karthik, S. Dhanuskodi, S. Prabu Kumar, C. Gobinath, S. Sivaramakrishnan, Mater. Lett. 206, 217 (2017) (doi:10.1016/j.matlet.2017.07.004).

С. Сакти Прайя[1], К. Балакрішнан[1], А. Лакшманан[1], П. Сурендран[1], П. Рамешкумар[1], Картік Каннан[2], П. Гіта[3], Теяшві Ашок Хегде[4], Г. Вініта[4]

Вирощування та характеристика монокристалів саліцилату бензимідазолію для нелінійних оптичних досліджень та антибактеріальної дії

[1]*Коледж Періяр Е. В. Р. (автономний), філія Університету Бхаратідасан, Тіручіраппаллі, Тамілнаду, Індія*, rameshkumarevr@gmail.com
[2]*Center for Advanced Materials, Катарський університет, поштова скринька 2713, Доха, Катар*, karthikkannanphotochem@gmail.com
[3]*Quaid-E-Millath урядовий коледж для жінок (автономний), Ченнаї 600002, Тамілнаду, Індія*, geethasuresh29081978@gmail.com
[4]*Школа передових наук, Технологічний інститут Vellore, Ченнаї, Тамілнаду 600127, Індія*, tejaswihegade4@gmail.com

Органічні нелінійні оптичні моноцитрали саліцилату бензимідазолію (BISA) отримували з розчину метанолу методом повільного випаровування. Вирощені кристали належать до *моноклінної* кристалічної системи з просторовою групою $P2_1/c$. Чітка кристалічна природа вирощеного кристалу BISA підтверджена PXRD. FTIR спектральний аналіз свідчить про наявність функціональних груп у кристалі BISA. Зі спектрів УФ – видимого діапазону поглинання розраховано нижню граничну довжину хвилі (356 нм), ширину забороненої зони та лінійний показник заломлення. Спектр люмінесценції реєстрували при дослідження піку випромінювання при 426 нм. Механічну міцність кристалу BISA визначено за допомогою тестера мікротвердості Віккерса і вперше розраховано такі механічні параметри, як C_{11}, H_k, K_c, and B_i. Діелектричні властивості вирощених кристалів систематично досліджували при різних температурах. Крім того, електронну поляризацію (α) розраховано за допомогою аналізу Пенна та рівняння Клаузіуса – Моссотті. Для вимірювання властивостей третього порядку NLO кристалу BISA застосовано Z – сканування. Вперше кристали BISA тестували на п'ять патогенних для людини бактерій, таких як *Bacillus cereus*, *Staphylococcus aureus*, *Shigella flexneri*, *Vibrio cholerae*, and *Klebsiella pneumoniae*. Отримані результати показали, що кристали саліцилату бензимідазолію можуть знайти корисне застосування в нелінійній оптиці та антимікробній галузі.

Ключові слова: вирощування кристалів, оптичні дослідження, діелектричні дослідження, Z-сканування, антибактеріальна активність.